Induced Point and Correlated Disorder Pinning in Untwinned $YBa_2Cu_3O_{7-\delta}$ Crystals

W.K. Kwok, L. Paulius[1], D. Lopez[2], H. Safar[2], R.J. Olsson[3], A.M. Petrean[1], and G.W. Crabtree

Materials Science Division and Science and Technology Center for Superconductivity
Argonne National Laboratory, Argonne, Illinois 60439

International Rare Earths Conference "98" Fremantle, Western Australia October 25-30, 1998

This work was supported by the U.S. Department of Energy, BES-Material Sciences, under Contract No. W-31-109-ENG-38, the NSF Office of Science and Technology Center for Superconductivity under Contract No. DMR91-20000, NSF-DMR96-24047 (LMP) and an NSF CAREER Award DMR-9702535 (HS).

[1]also at Dept. of Physics, University of Western Michigan, Kalamazoo, MI, USA
[2]Dept. of Physics, University of Illinois at Chicago, Chicago, IL, USA
[3]also at Dept. of Physics, Michigan State University, East Lansing MI, USA

DISCLAIMER

Induced Point and Correlated Disorder Pinning in Untwinned $YBa_2Cu_3O_{7-d}$ Crystals

W. K. Kwok, L. Paulius*, D. Lopez+, H. Safar+, R. J. Olsson&, A. M. Petrean*, and G. W. Crabtree.

Materials Science Division and Science and Technology Center for Superconductivity, Argonne National Laboratory, Argonne, IL 60439, USA

Abstract

Keywords: superconductivity, vortex pinning

The magnetic phase diagram of untwinned single crystals of $YBa_2Cu_3O_{7-\delta}$ is studied via transport measurements. We show that the first order vortex melting line which terminates at a critical point in high magnetic fields is strongly dependent on point disorder induced by proton irradiation. In addition, we report on the effect of heavy ion irradiation induced columnar defects on vortex pinning.

The rich magnetic phase diagram of high temperature superconductors has been investigated extensively in recent years. One of the salient features of the T_{co}~90K high temperature superconductor, $YBa_2Cu_3O_{7-\delta}$ (YBCO), is a first order phase transition from a vortex lattice state to a vortex liquid state. This transition has been investigated with both dynamic[1-4] and thermodynamic measurements[5-7]. The vortex melting transition occurs at magnetic fields well below the upper critical field, resulting in a large portion of the magnetic phase diagram where the vortex lattice is melted and in the liquid state. At high magnetic fields, the melting line terminates at a critical point[8,9], above which the transition is purported to be continuous.

The variety of vortex phases is demonstrated by the type and dimensionality of the defects. In samples with a high density of point defects, a vortex glass phase[10] has been predicted. In systems with correlated defects like twin boundaries or columnar defects, a Bose glass state[11] has been predicted. In addition, if the vortex liquid state consists of topologically entangled vortices, a continuous transition to a polymer glass state at low temperatures may not be ruled out[12]. Techniques have been developed to incorporate point defects and correlated defects in a controlled manner into these materials via electron, proton and heavy ion irradiation. However, if the reference material has inherent defects, it is difficult to isolate the induced pinning effects from the inherent behavior. Experiments on clean crystals with a first order

vortex melting transition allow for a better understanding of the effect of defects in high temperature superconductors.

Proton Irradiation

A twinned platelet YBCO crystal with dimensions 2000μm x 500μm x 150μm was grown by the self-flux method. The crystal was detwinned by applying uniaxial pressure parallel to the ab-plane. Polarized light microscopy showed no signs of twin planes after the detwinning process. Eight electrical gold contacts were evaporated onto the top and bottom of the crystal in the modified flux transformer configuration[13]. Gold wires were attached to the crystal with silver epoxy, resulting in contact resistance of about 1Ω. Half of the crystal was irradiated with 9 MeV protons to a dose of 1 x 10^{15} /cm^2 while the other half was shielded with a tantalum mask and used as a reference. From TRIM[13] calculations, this gives a defect spacing of approximately 88Å assuming no annealing or clustering of point defects. Transport measurements were performed using the standard four probe method with both ac and dc techniques in magnetic fields up to 18T at the Los Alamos High Magnetic Field Laboratory. The unirradiated portion of the crystal exhibited a zero field transition temperature of T_{co}=93.25K with width ΔT_{co}<300mK, underlining the high quality of the sample.

Figure 1 shows the temperature dependence of the resistance in magnetic fields from zero to 18 Tesla. The sharp kink in the tail of the resistive transition, observed between H=1T and 12T, is associated with the first order vortex solid to liquid phase transition[4]. At high fields above H=12T, the kink in the resistance curve rapidly decreases. At H=14T, a small vestige of the sharp drop is still observable near T=71K, but at H=16T, the kink is completely suppressed. The inset shows the temperature derivative of the resistance curves for H=12T and 18T. The sharp peak in dR/dT is used to identify the vortex lattice melting temperature T_m. The peak is virtually absent for H=18T compared to the

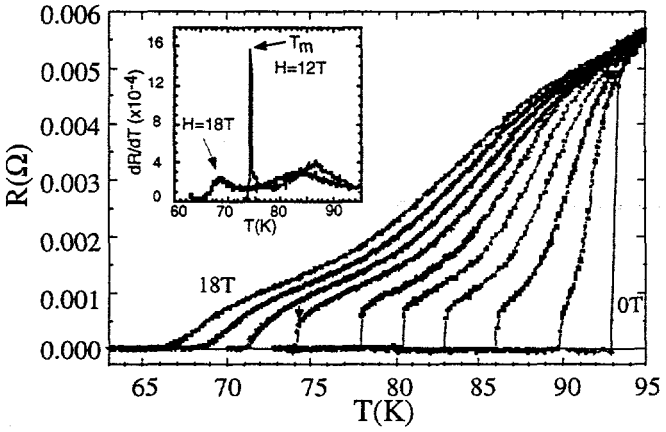

Figure 1. The resistive transition in magnetic fields of 0, 1, 3, 5, 7, 9, 12, 14, 16, and 18Tesla parallel to the c-axis. The inset shows the temperature derivative of the resistance for 12 and 18T.

H=12T data. From these measurements, we determined the vortex melting line shown by the open circles in figure 2. The line can be fitted to $H_m=110(1-T/T_{co})^{1.39}$, consistent with values reported on high quality untwinned crystals[2]. The critical point is identified by the lack of a sharp kink in the resistance curve and occurs near $H_{cp}=12.5T$. The closed circles identify the continuous transition line at high fields above the critical point.

Similar measurements and analysis were carried out for the proton irradiated portion of the crystal. Since the defect spacing is about 88Å, the low density of irradiation induced point defects was not sufficient to completely suppress the first order vortex melting transition. Instead, the maximum magnetic field where the kink occurred was decreased. The vortex lattice melting line for the irradiated portion of the crystal is shown by the open squares in figure 2. The melting line for the irradiated crystal follows the melting line of the unirradiated crystal. However, the critical point is depressed along the melting line from $H_{cp}=12.5T$ for the unirradiated crystal to about $H_{cp}=9T$ for the irradiated portion of the crystal.

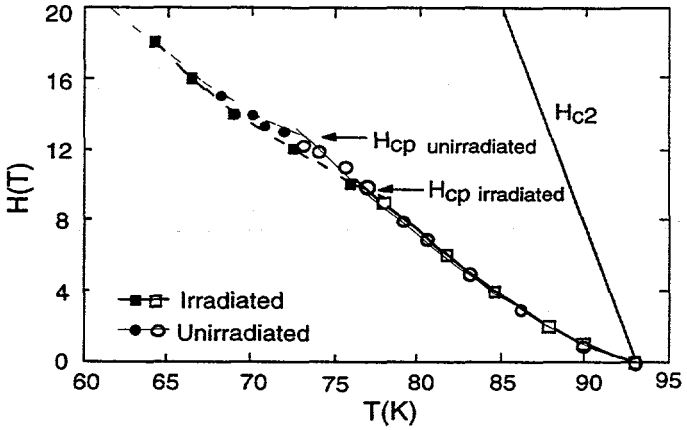

Figure 2. Magnetic phase diagram of YBCO before and after proton irradiation .

Our results demonstrate that the critical point is strongly dependent on point disorder. The nature of the continuous transition above the critical point has not yet been established. We did not find vortex glass scaling behavior above the critical point. A sufficient irradiation dose that will completely suppress the first order melting transition may be required for the vortex glass solid state to materialize.

Uranium Heavy Ion Irradiation

Amorphous linear tracks or columnar defects in high temperature superconductors, created by high energy heavy ion irradiation have so far yielded the most noteworthy vortex pinning enhancement by shifting the irreversibility line to higher temperatures and increasing the critical current at both high temperatures and high fields[14-16]. The advantage of this method of introducing correlated defects is that

vortex pinning can be controlled by the irradiation dose, which can be related to a dose equivalent 'matching field' B_Φ where the number of columnar defects equals the number of vortices. Thus the magnetic field range over which pinning is enhanced can be tailored. Most previous experiments on the effect of heavy ion irradiation in YBCO have been performed on twinned single crystals. Since twin boundaries can also act as a correlated pinning site[17], they can compete with the induced columnar defects, complicating the separation of the two contributions to vortex pinning. Using untwinned crystals eliminates the interfering effects from twin boundaries.

We carried out a systematic investigation of the effect of dose matching field on a large untwinned YBCO crystal that was cleaved into five pieces. Three of the pieces were irradiated with 1.4GeV $^{238}U^{67+}$ ions to a matching field of B_Φ=1T, 2T, and 4T, equivalent to a dose of $n=B/\Phi_o$= 4.8 x $10^{14}m^{-2}$, 9.6 x $10^{14}m^{-2}$, and 1.9 x $10^{15}m^{-2}$ respectively, where Φ_o =2.07 x 10^{-15} T-m^2 is the flux quantum. This method guarantees that all three crystals have the same underlying reference state. High energy uranium ions impinging on the samples create an amorphous columnar defect with a diameter of about 50Å to 100Å. Since the size and dimensionality is comparable to the size of the vortex core $\xi(T)$ near T_{co}, pinning is believed to be quite effective. The zero field resistive transitions of the three crystals are shown in figure 3. Before irradiation, the zero field transition temperature of the crystal was T_{co}=92.66K, determined from the peak in the temperature derivative of the resistivity, $d\rho/dT$. After irradiating the crystals to a matching field of B_Φ=1.0T, 2.0T, and 4.0T, the superconducting temperature decreased to 90.84K, 89.71K and 88.57K respectively. The normal state resistivity also increased with irradiation dose. An increase in the normal state resistivity near T=100K of about 16% is observed between the unirradiated and the B_Φ=1T irradiated crystal. On the other hand, crystals irradiated with B_Φ=2T and 4T showed larger increases in the normal state

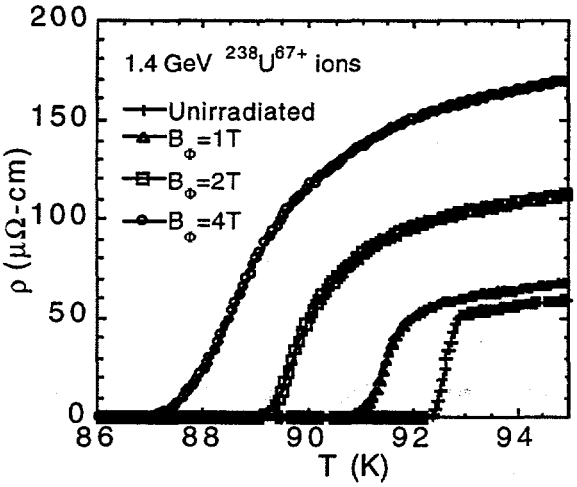

Figure 3. Zero field resistivity versus temperature for B_Φ=0, 1, 2, 4 Tesla

resistivity and the width of the zero field resistive transition. This is attributed to the large damage inflicted upon the sample at these high dose. For example, a dose of B_Φ= 4T produces a columnar defect spacing of about 220Å apart. Since the columnar defect cores are about 100Å in diameter, this gives a separation between the perimeter of the columnar defects of only 120Å. Furthermore, it has been shown that recrystallization[18] and strain fields may occur near the edges of the columnar defects leading to an even wider damage area.

The normalized resistivity as a function of temperature for various different magnetic fields parallel to the crystallographic c-axis and the ab-plane is shown in figure 4. The pre-irradiation resistivity curves show a sharp 'kink' in the resistive transition associated with the first order vortex melting transition for both H || c and H || b. After irradiation with B_Φ=1, 2, and 4T, the kink in the resistivity curve is completely suppressed and replaced with a smooth curve. The normalized zero resistance temperature of the irradiated crystals shifts to higher temperature with increasing irradiation dose for H || c, while the opposite is observed for H || b.

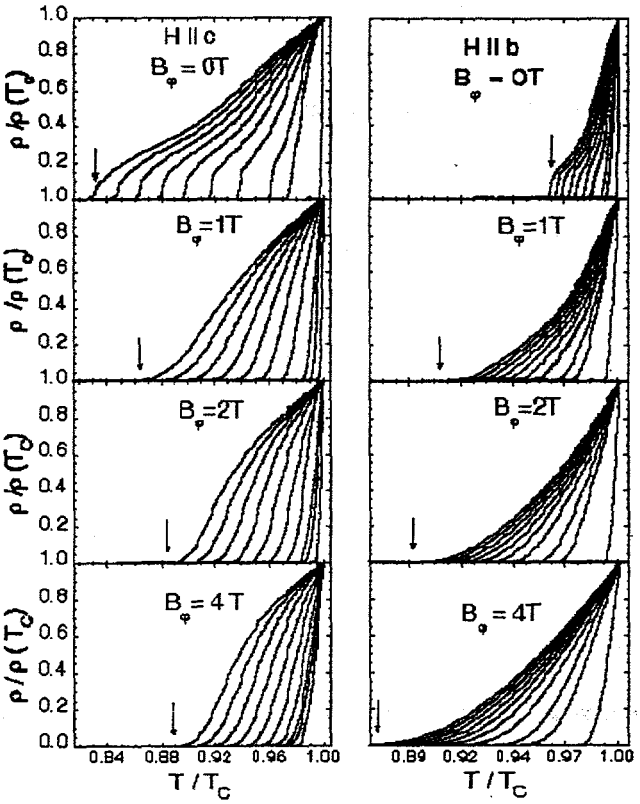

Figure 4. Normalized resistivity versus temperature for H=0, 0.5, 1, 2, 3, 4, 54, 6, 7, 8T || c and || b

The vortex lattice melting line for the unirradiated crystal is shown in figure 5a. The pre-irradiation melting line for H || c can be fit to H_m=88.4 $(1-T/T_{co})^{1.36}$, consistent with other high quality single crystals of YBCO. After irradiation, the first order vortex melting line is completely suppressed. Therefore we define an irreversibility line from the zero resistivity temperature using a criterion of ρ=0.01$\mu\Omega$-cm, the resolution of our equipment. A comparison of the $H_{irr}(T)$ || c curves of the irradiated crystals is shown in figures 5(a-c) and delineates a distinct change in slope at the dose matching field B_Φ. For B_Φ=1T, the irreversibility line for

H || c follows a linear behavior above H=1.0T and a sharp upward curvature below 1T. Likewise, for B_Φ=2T and 4T, a change in slope of the $H_{irr}(T)$ || c is observed near H=2T and 4T respectively. This change is slope indicates a change in vortex pinning behavior. Below H=B_Φ, there are more columnar defects than vortices, and each vortex can be pinned by a columnar defect. The irreversibility line is represented by a rapid concave upward rise. However, for H > B_Φ, interstitial vortices begin to appear since all the columnar defect pinning sites may be occupied by a vortex line and thus the sharp rise in the irreversibility line is replaced by a linear behavior with a smaller slope. The fact that we observe this change in behavior very close to the dose matching field attests to the high control over the density of induced columnar defects.

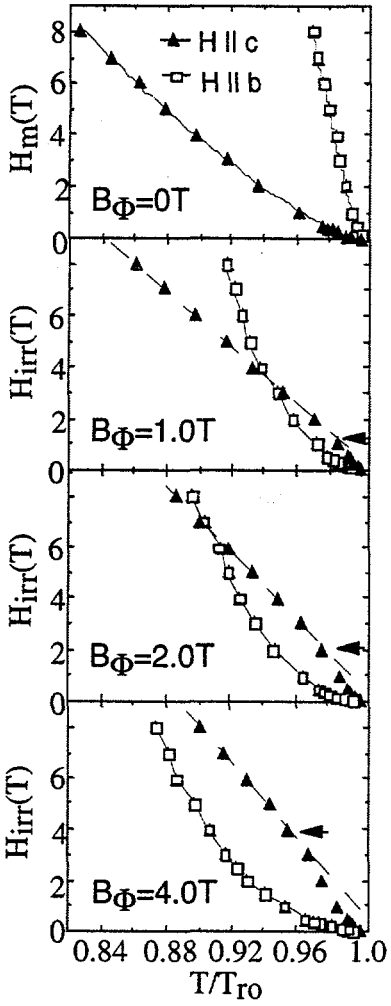

Figure 5: (a) Melting line of unirradiated crystal; (b) Irreversibility line for B_Φ=1.0T crystal; (c) B_Φ=2.0T crystal; and (d) B_Φ=4.0T crystal for H || c and H || b.

The remarkable result is the crossing of the $H_{irr}(T)$ || c and $H_{irr}(T)$ || b lines at magnetic fields about three times the matching field. For B_Φ=1.0T and 2T, the crossing occurs near 3.3T and 6.8T respectively. For B_Φ=4T, a linear extrapolation yields a crossing near 12.5T. The irreversibility line for H || b lies below the H_{irr} || c curve below about 3.3 B_Φ. Our results suggest that columnar defects along the c-axis, may act as conduits for easy vortex motion when the magnetic field lines are aligned perpendicular to the columnar defects. In our measurements, the transport current, J || a, is perpendicular to the applied magnetic field. Thus for H || b, the Lorentz force exerted on the vortices by the magnetic field and current is on average, along the c-axis. We have previously shown that intrinsic pinning due to the layered structure is responsible for localizing the vortices in the ab-plane[19]. The induced columnar defects drilled through the layered structure of the crystal may suppress intrinsic pinning by introducing a new channel for vortex creep motion between the layers. At high fields

above $3.3B_\Phi$, point defects may eventually dominate over the correlated defects leading to the crossing of the $H_{irr} \parallel c$ and $H_{irr} \parallel b$ irreversibility lines.

Finally, anisotropic vortex pinning by correlated defects is demonstrated in figure 6. The top panel shows the angular dependence of the resistivity at H=0.5T at various temperatures for the unirradiated crystal. The inherent anisotropy of the crystal, is clearly observed here where a maximum in dissipation occurs at H || c and a minimum at H || b. The angular dependence of the resistivity after irradiation with a dose matching field of B_Φ=2T is shown in the bottom panel. The maximum dissipation at θ=0° (H || c) is now replaced with a minimum. The maximum dissipation occurs at about 70° from the c-axis. From these measurements, we can define a depinning angle θ_{depin}, beyond which the columnar defects are no longer effective in pinning the vortex line along its entire length. Notice that the data are plotted in reduced temperatures $t=T/T_{co}$. The onset of the minimum at θ=0° begins very close to t=1, and points to the high vortex *liquid* pinning capability of these columnar defects.

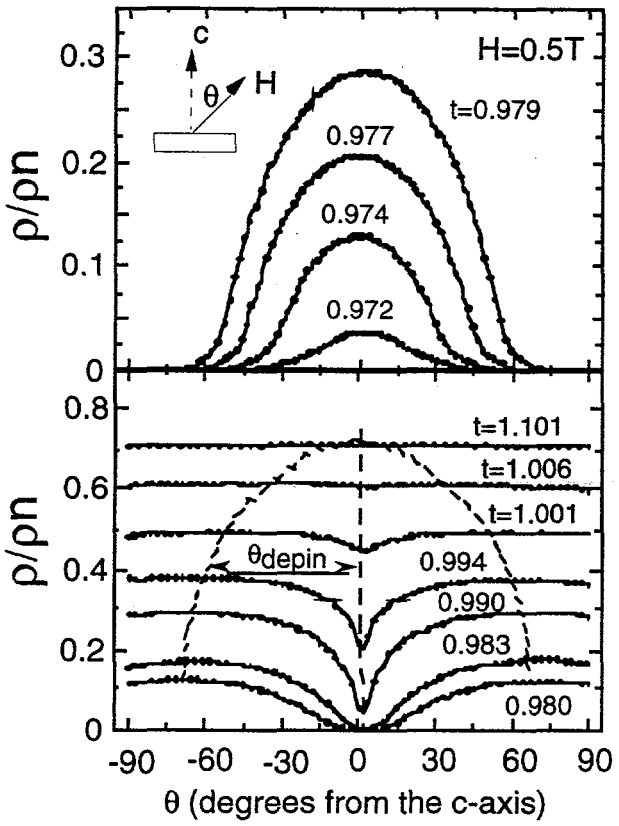

Figure 6: Angular dependence of the resistivity for an untwinned (a) unirradiated and (b) heavy ion irradiated YBCO crystal

In summary, we found that the critical point is very sensitive to point disorder. Increasing the point disorder can shift the critical point down along the first order vortex melting line. For columnar defects, the first order vortex melting line is completely suppressed and replaced by a continuous transition line. We found a consistent change in the slope of the irreversibility line at the matching field and a remarkable reversal of the pinning anisotropy. Finally, anisotropic pinning from columnar defects induced by uranium heavy ions can extend up to T_{co}, suggesting that

even in the superconducting fluctuation regime, these defects are capable of pinning the vortex liquid.

Acknowledgement

This work was supported by the U. S. Department of Energy, BES-Material Sciences, under Contract No. W-31-109-ENG-38, the NSF Office of Science and Technology Center for Superconductivity under Contract No. DMR91-20000, NSF-DMR96-24047 (LMP) and an NSF CAREER Award DMR-9702535 (HS).

References

* also at Dept. of Physics, University of Western Michigan, Kalamazoo MI, USA
+ Dept. of Physics, University of Illinois at Chicago, Chicago IL, USA
& also at Dept. of Physics, Michigan State University, East Lansing MI, USA

1. H. Safar et al., Phys. Rev. Lett. 69, 824 (1992)
2. W. K. Kwok et al., Phys. Rev. Lett. 69, 3370 (1992); ibid. Phys. Rev. Lett. 72, 1092 (1994).
3. M. Charalambous et al., Phys. Rev. B 45, 5091 (1992).
4. J. Fendrich et al., Phys. Rev. Lett. 77, 2073 (1996).
5. R. Liang et al., Phys. Rev. Lett. 76, 835 (1996).
6. U. Welp et al., Phys. Rev. Lett. 76, 4809 (1996);
7. A. Schilling et al., Nature 382, 791 (1996); ibid. Phys. Rev. Lett. 78, 4833 (1997).
8. H. Safar et al., Phys. Rev. Lett. 70, 3800 (1993).
9. D. Lopez et al., Phys. Rev. Lett. 80, 1070 (1998).
10. D. S. Fisher, M. P. A. Fisher, and D. Huse, Phys. Rev. B43, 130 (1991)
11. D. R. Nelson and V. M. Vinokur, Phys. Rev. Lett. 68, 2398 (1992).
12. J. Fendrich et al., Phys. Rev. Lett. 74, 1210 (1995).
13. J. P. Biersack and J. F. Ziegler, Transport of Ions in Matter (TRIM)-Monte Carlo Simulation Program, Ver.91.14.
14. L. Civale et al., Phys. Rev. Lett. 67, 648 (1991).
15. M. Konczykowski et al., Phys. Rev. B 44, 7167 (1991).
16. L.M. Paulius et al., Phys. Rev. B 56, 913 (1997).
17. S. Fleshler et al., Phys. Rev. B 47, 14448 (1993).
18. Y. Yan and M. A. Kirk, Phys. Rev. B57, 6152 (1998).
19. W. K. Kwok et al., Phys. Rev. Lett. 72, 1088 (1994).